

TRANSFORMATION OF MORPHOLOGY AND LUMINOSITY CLASSES OF THE SDSS GALAXIES

CHANGBOM PARK¹, J. RICHARD GOTT III², & YUN-YOUNG CHOI¹

Draft version November 9, 2018

ABSTRACT

We present a unified picture on the evolution of galaxy luminosity and morphology. Galaxy morphology is found to depend critically on the local environment set up by the nearest neighbor galaxy in addition to luminosity and the large scale density. When a galaxy is located farther than the virial radius from its closest neighbor, the probability for the galaxy to have an early morphological type is an increasing function only of luminosity and the local density due to the nearest neighbor (ρ_n). The tide produced by the nearest neighbor is thought to be responsible for the morphology transformation toward the early type at these separations. When the separation is less than the virial radius, i.e. when $\rho_n > \rho_{\text{virial}}$, its morphology depends also on the neighbor's morphology and the large-scale background density over a few Mpc scales (ρ_{20}) in addition to luminosity and ρ_n . The early type probability keeps increasing as ρ_n increases if its neighbor is an early morphological type galaxy. But the probability decreases as ρ_n increases when the neighbor is a late type. The cold gas streaming from the late type neighbor can be the reason for the morphology transformation toward late type. The overall early-type fraction increases as ρ_{20} increases when $\rho_n > \rho_{\text{virial}}$. This can be attributed to the hot halo gas of the neighbor which is confined by the pressure of the ambient medium held by the background mass. We have also found that galaxy luminosity depends on ρ_n , and that the isolated bright galaxies are more likely to be recent merger products. We propose a scenario that a series of morphology and luminosity transformation occur through distant interactions and mergers, which results in the morphology–luminosity–local density relation.

Subject headings: galaxies:general – galaxies:formation – galaxies:evolution – galaxies:morphology – galaxies:luminosity

1. INTRODUCTION

Diverse galaxy morphology is one of the cosmological mysteries in which the secret of structure formation and evolution might be hidden. Galaxy morphology is known to be correlated with luminosity and spatial environment, and there is a hope that knowledge on the correlations among them may provide clues to unravel the mystery. This line of study began in the 1930's. Hubble & Humason (1931) found that clusters were dominated by ellipticals and lenticulars and that environmental factors played an important role in determining the morphology of galaxies. Oemler (1974) found the morphology-radius relation; the late type galaxy fraction decreases with radius within a cluster. This relation was confirmed by Dressler (1980) who argued that the fraction of morphological types is a function of local galaxy density. Postman & Geller (1984) extended this morphology-density relation down to the group environment. On the other hand, galaxy luminosity is also known to depend on environment. An excess of bright galaxies in clusters has been pointed out by Schechter (1976). It is now well-accepted that both amplitude and shape of the luminosity function of the individual morphological types vary with environment (Park et al. 2007). Despite these empirically known relations, it is very complicated to disentangle independent factors from the interrelations among various physical parameters of galaxies and environment.

On the theoretical side, there have been many ideas

about the mechanisms causing such observational effects. Gunn & Gott (1972) argued that S0 galaxies in great relaxed clusters like Coma were the result of spirals being stripped of gas by ram pressure stripping due to hot intra-cluster gas. High speed encounters of galaxies with other halos typically in clusters cause impulsive heatings, called harassment (Moore et al. 1996), and can transform spirals to early types. Strangulation (Balogh, Navarro & Morris 2000) is another mechanism that can also transform morphology through decline of the star formation rate (SFR) due to shut-off of the newly accreted gas when a galaxy enters a cluster or group environment and loses its hot gas reservoir. There is also observational and theoretical evidence that the general tidal force field in clusters can transform infalling spirals to early types (Moss & Whittle 2000; Gnedin 2003). It is also plausible for galaxy morphology to be largely determined by the initial conditions when galaxies were formed. Gott & Thuan (1976) argued that elliptical galaxies were produced by a larger initial density which would have higher density at turn-around and where star formation would be completed before collapse. Such larger initial density would be more likely in a region that would later turn into a high density environment.

It is important to note that all the nurture processes proposed so far are basically effective in group or cluster environments. However, there seems to be morphology and luminosity-determining processes which work at all local densities in a continuous way. This is supported by the fact that there is no feature in the galaxy property versus local density relation at any local density when morphology is fixed (Park et al. 2007). But it was found that the fraction of late morphological type

¹ Korea Institute for Advanced Study, Dongdaemun-gu, Seoul 130-722, Korea; cbp@kias.re.kr, yychoi@kias.re.kr

² Department of Astrophysical Sciences, Peyton Hall, Princeton University, Princeton, NJ 08544-1001, USA

decreases sharply above the critical luminosity of about $M_r = -21.3 + 5\log h$ in the morphology versus luminosity relation (Choi et al. 2007, hereafter Paper I).

Recently, the Two Degree Field Galaxy Redshift Survey (2dFGRS; Colless et al. 2001) and the Sloan Digital Sky Survey (SDSS; York et al. 2000) have been extensively used to accurately measure the environmental effects on various physical properties of galaxies (Goto et al. 2003; Balogh et al. 2004a,b; Blanton et al. 2005a; Croton et al. 2005; Tanaka et al. 2004; Weinmann et al. 2006; among many others). In this paper, we extend our work in companion papers which studied the relations among various physical properties of galaxies in the SDSS spectroscopic sample (Paper I), and the environmental dependence of the physical parameters (Park et al. 2007, hereafter Paper II). In particular, we will further inspect the findings that galaxy morphology varies with both the density measured on a few Mpc scales and the distance to the nearest bright galaxy, and that the dependence of the early-type fraction on the nearest neighbor distance is strongest when the distance is about $200h^{-1}$ kpc. It will be shown that this separation corresponds to the virial radius of the typical galaxies used in the study. We will perform an extensive study of the dependence of galaxy morphology on luminosity, large-scale density, the local density due to the closest neighbor, and morphology of the neighbor. Galaxy morphology is found to depend on the various local environment parameters in a more complicated way. Taking into account the fact that galaxy morphology is closely related with luminosity, we extended our work to inspect the morphology transformation in conjunction with luminosity class transformation of galaxies. For this purpose, we use large volume-limited samples divided into accurate morphological subsets of early and late type galaxies in several luminosity bins.

2. OBSERVATIONAL DATA SET

2.1. Sloan Digital Sky Survey Sample

We use a large-scale structure sample, DR4plus (LSS-DR4plus), of the SDSS (York et al. 2000; Blanton et al. 2003a; Fukugita et al. 1996; Gunn et al. 1998, 2006; Hogg et al. 2001; Ivezić et al. 2004; Lupton et al. 2001; Pier et al. 2003; Smith et al. 2002; Stoughton et al. 2002; Tucker et al. 2006) from the New York University Value-Added Galaxy Catalog (NYU-VAGC; Blanton et al. 2005b). This sample is a subset of the SDSS Data Release 5 (Adelman-McCarthy et al. 2007). Our major sample of galaxies used here is the LSS-DR4plus sample referred to as “void0,” which includes the Main galaxies (Strauss et al. 2002) with the r -band apparent magnitudes in the range $14.5 < r_{\text{Pet}} < 17.6$ and redshift in the range $0.001 < z < 0.5$. For the approximately 6% of targeted galaxies that lack a measured redshift because of fiber collisions, we assign the redshift of the nearest neighbor.

The r -band absolute magnitude $^{0.1}M_r$ used in this study is the AB magnitude converted from SDSS magnitudes. To compute colors, we use extinction (Schlegel et al. 1998) and K-corrected model magnitudes. The superscript 0.1 means the rest-frame magnitude K-corrected to redshift of 0.1 (Blanton et al. 2003b). All of our magnitudes and colors follow this convention, and the

superscript will be subsequently dropped. We also drop the $+5\log h$ term in the absolute magnitude. We use the luminosity evolution correction of $E(z) = 1.6(z - 0.1)$ (Tegmark et al. 2004). We adopt a flat Λ CDM cosmology with $\Omega_\Lambda = 0.73$ and $\Omega_m = 0.27$.

Completeness of the SDSS is poor for bright galaxies with $r < 14.5$ because of spectroscopic selection criteria (which exclude objects with very large flux within the fiber aperture) and difficulties of automatically measuring photometric properties of very extended sources. As described in detail in section 2.1 of Paper I, we add the missing bright galaxies and thereby extend the magnitude range by using various existing redshift catalogs which we match to the SDSS data. In total, 5195 bright galaxies are added to the void0 samples within our angular sample boundaries (see Fig. 1 of Paper II). Volume-limited samples derived from the resulting catalog have nearly constant comoving number density of galaxies in the radial direction for redshifts $z \geq 0.025$. We treat our final sample as effectively having no bright limit at redshifts greater than $z = 0.025$. More details about this sample can be found in Paper I.

To study the effects of environment on galaxy properties it is advantageous for the observational sample to have the lowest possible surface-to-volume ratio, so that boundary effects are minimized (see Park et al. [2005] regarding similar effects in a topology analysis). For this reason we trim the DR4plus sample as shown in Figure 1 of Paper II. The three stripes in the Southern Galactic Cap observed by SDSS are not used because of their narrow angular extent. These cuts leave approximately 4464 deg^2 in the survey region. Within our sample boundaries, we account for angular variation of the survey completeness by using the angular selection function defined in terms of spherical polygons (Hamilton & Tegmark 2004), which takes into account the incompleteness due to mechanical spectrograph constraints, bad spectra, or bright foreground stars. The resulting useful area (with nonzero selection function) within the analysis regions is 1.362 sr. In our study it is very important to use volume-limited samples of galaxies that maintains uniform sampling in space and luminosity. The absolute magnitude and redshift limits of a set of our volume-limited samples are shown in Figure 2 of Paper I. The definitions for the samples are summarized in Table 1. We mainly use the $D4$ sample which includes 74,688 galaxies with $M_r \leq -19.5$. The $D5$ sample, used in Figure 5, includes 80,479 galaxies with $M_r \leq -20.0$.

2.2. Morphology Classification

An important feature of this work is the use of large, accurate morphology subsets. We first classify morphological types of galaxies using the prescription of Park & Choi (2005). Galaxies are divided into early (ellipticals and lenticulars) and late (spirals and irregulars) morphological types based on their locations in the $u-r$ color versus $g-i$ color gradient space and also in the i -band concentration index space. Our study is about the morphological transformation between the early and late types, and not within the subclasses. To measure the color gradient and the concentration index, we use the g - and i -band atlas images and employ basic photometric parameters measured by the Princeton/NYU

TABLE 1
VOLUME-LIMITED SAMPLES

Name	Absolute Magnitude	Redshift	Distance ^a	Galaxies
D3	$M_r < -19.0$	$0.025 < z < 0.06869$	$74.6 < R < 203.0$	49571
D4	$M_r < -19.5$	$0.025 < z < 0.08588$	$74.6 < R < 252.9$	74688
D5	$M_r < -20.0$	$0.025 < z < 0.10713$	$74.6 < R < 314.0$	80479

^aComoving distance in units of h^{-1} Mpc

group ³. The boundaries between the two types in the three-dimensional parameter space is determined in such a way that the classification best reproduces the visual morphology classification. The resulting morphological classification has completeness and reliability reaching 90%, as claimed by Park & Choi (2005). When photometry is excellent and galaxy images are well-resolved, more information from surface brightness fluctuations can be added for morphology classification. But this is certainly not the case near the faint limit ($r = 16.5 \sim 17.6$) of the SDSS sample we use.

Our automatic classification scheme does not perform well when an early type galaxy starts to overlap with other galaxy. This is because the scheme excludes galaxies with very low concentration from the early type class and blended images often erroneously give low concentration. Since we are investigating the effects of close pairs on galaxy luminosity and morphology, this problem in the automatic classification has to be remedied. In the case of the volume-limited sample D4 we perform an additional visual check of the color images of galaxies to correct misclassifications by the automated scheme for about 20,000 galaxies located at the local density $\rho_n/\bar{\rho} > 100$ (see below for the definition of ρ_n). In this procedure we changed the types of the rare galaxies which are blue but elliptical galaxies, blended or merging ones, or dusty edge-on spirals. Some non-sense objects are removed from the samples, and those with wrong central positions are corrected.

2.3. Local environment

To find relations between intrinsic physical properties of galaxies and their environment we require a well-defined and robust measure of environment. We seek to use environmental parameters that are defined directly from observational data, and characterize the full range of galaxy environments, from the most massive clusters to voids. Most previous studies have used the local galaxy number density as a measure of local environment. In the present study we will consider three kinds of environment. One is the mass density described by many neighboring galaxies over a few Mpc scale. This is called the large-scale background density. Another is the local mass density attributed to the closest neighbor galaxy. The third is the morphology of the closest neighbor galaxy.

The background density at a given location of a galaxy is measured by

$$\rho_{20}(\mathbf{x})/\bar{\rho} = \sum_{i=1}^{20} \gamma_i L_i W_i(|\mathbf{x}_i - \mathbf{x}|)/\bar{\rho}, \quad (1)$$

³ <http://photo.astro.princeton.edu>

using the luminosity L of the closest twenty galaxies in a volume-limited sample. Here the mass associated with a galaxy is assumed to be proportional to the luminosity of the galaxy. The mean mass density within a sample of the total volume V is obtained by

$$\bar{\rho} = \sum_{\text{all}} \gamma_i L_i / V, \quad (2)$$

where the summation is over all galaxies in the sample. The mean density of each volume-limited sample is nearly a constant when the magnitude limit of the sample is fainter than $M_r = -19.5$. Only the relative mass-to-light ratios (γ) for early and late types are needed. We assume $\gamma(\text{early}) = 2\gamma(\text{late})$ at the same r -band luminosity. This is our choice of the connection between luminosity and morphology with the host halo mass. It is based on the fact that the central velocity dispersion of early type galaxies brighter than about $M_r = -19.5$ is about $\sqrt{2}$ times that of late types (Fig. 4b of Paper I). It is also consistent with our finding that the RMS velocity difference between a galaxy and its neighbor galaxies is about 1.5 larger for the early types (see section 2.4). We find the mean mass density

$$\bar{\rho} = 0.0223 \pm 0.0005(\gamma L)_{-20}, \quad (3)$$

where $(\gamma L)_{-20}$ is the mass of a late-type galaxy with $M_r = -20$. We use the spline-kernel weight $W(r)$ for the background density estimation as in Paper II. We vary the size of the spline kernel, h_s , to include a fixed number of galaxies within the kernel weighting. This adaptive smoothing kernel is often used in smoothed particle hydrodynamics simulations. We use the spline kernel because it is centrally weighted, unlike the tophat or cylindrical kernel, and has a finite tail, unlike the Gaussian.

Because this smoothing kernel is adaptive and centrally weighted, it has the important feature that it does not oversmooth dense regions, thereby blurring the ‘walls’ into the ‘voids’. Maps of the observed redshift space distribution of galaxies support this picture (see Fig. 3 of Paper II). The adaptive nature of the smoothing kernel makes the physical smoothing scale systematically vary with environment, from a small smoothing scale in clusters to a very large smoothing scale in voids. Since the high density regions collapse while the under dense regions expand as the universe evolves, the adaptive kernel allows more uniform smoothing scale in the ‘initial’ conditions compared to the method adopting a fixed-scale at the present epoch.

In our study the number of galaxies required within the smoothing volume is set to $N_s = 20$, which we find is close to the smallest number yielding good local den-

sity estimates. When searching for the spline radius containing the required number of galaxies, the smoothing volume can hit the sample boundaries or masked regions due to bright stars or galaxies. In addition to this trouble, the angular selection function varies across the sky even within the survey region. We first check if the location where the background density is being measured is within the survey area, and then ignore the survey geometry and angular selection function to search for the nearest 20 galaxies in order to find the spline radius and thus the local density using equation (1). We then randomly throw 1000 test particles into the smoothing volume around the location, and calculate the sum of normalized weights of the test particles assigned by the spline kernel, the angular selection function, and the radial boundaries. The final local density is given by the first estimate divided by the sum of weights.

We have estimated the accuracy of the ρ_{20} measure of the background density. We identified dark halos with mass more than about $1 \times 10^{12} h^{-1} M_{\odot}$ (Kim & Park 2006) from a large Λ CDM N-body simulation using 2048³ particles made by Park et al. (2005), and measured the dark halo number density ρ_{20} in real and redshift spaces. The error in the redshift space ρ_{20} is found to be 12 and 31% at densities $\rho_{20}/\bar{\rho} = 0.5$ and 10, respectively.

In Paper II, only the L_* galaxies with $M_r = -20 \sim -21$ were used to trace the number density field. The background density ρ_{20} here differs from that of Paper II in that it represents the mass density rather than the number density and that the density tracers include all galaxies brighter than the faint magnitude limit of a sample. As a result, ρ_{20} distinguishes high density regions from low density regions much better. When the D4 sample is analyzed, the galaxies tracing the mass density are all galaxies brighter than $M_r = -19.5$. The median radius of the smoothing kernel is $h_S = 2.96 h^{-1}$ Mpc and its 68% limits are $h_S = 1.96$ and $4.38 h^{-1}$ Mpc.

The small-scale density experienced by a target galaxy located at \mathbf{x} is estimated by

$$\rho_n(\mathbf{x})/\bar{\rho} = 3\gamma_n L_n / 4\pi r_p^3 \bar{\rho}, \quad (4)$$

where r_p is the projected separation of the nearest neighbor galaxy from the target galaxy. The density due to the nearest neighbor used in our work does not represent the small-scale galaxy number density, but rather the local mass density given by the nearest neighbor itself. The method to find the nearest neighbor is described in the next section. Besides the nearest neighbor in terms of separation, we also adopted the neighbor galaxy giving the maximum value of ρ_n or the galaxy causing the maximum tidal energy deposit per unit mass (Binney & Tremaine 1987). We use a formula for the tidal energy deposit per unit mass

$$\Delta e \propto M_n^2 a^2 / \Delta v_n^2 (r_p^2 + a^2)^2, \quad (5)$$

where M_n is the mass of the neighbor, Δv_n is the velocity difference, and the size (the RMS radius) of the target galaxy a is set to 10 times the Petrosian radius. This combines the formulae for distant and penetrating encounters. When we used these criteria to choose the neighbor, our results were essentially the same. This is because the closest neighbors still dominate the latter two cases. The fraction of neighbors selected differently in these three nearest neighbor selection schemes is only

about 15%. We therefore present our results using only ρ_n of the nearest neighbor.

About 6% of galaxies in our samples missed the spectroscopic fibers due to the minimum fiber separation of $55''$ per tiling in the SDSS. When we estimated ρ_{20} or ρ_n , we included those galaxies with borrowed redshifts from the nearest neighbor on the sky. To estimate the errors in ρ_{20} and ρ_n due to this treatment we artificially increased the fraction of galaxies with borrowed redshifts in our sample and compared the results with the original density estimates. We first selected the galaxies who have measured redshifts and have neighbors within $55''$. The redshift of the nearest neighbor which has a measured redshift is assigned to these galaxies, neglecting their own redshifts so that a total of 6% of all galaxies in the sample D4 received new redshifts by this procedure. We found the ratio of ρ_{20} calculated from the degraded sample to the original density had 1.00 ± 0.12 , 1.01 ± 0.15 , and 1.04 ± 0.21 when $\rho_{20}/\bar{\rho} \leq 3$, $3 \sim 20$, and ≥ 20 , respectively. This tells that assigning the nearest neighbor's redshift makes ρ_{20} slightly overestimated in high density regions, and the scatter is between 10 ~ 20%. This error is less than that due to the redshift space distortion. We also checked the fraction of the nearest neighbors that were selected differently in the degraded sample. It is found that 15 and 7% of the nearest neighbors are selected differently for the pairs with separations less than 0.1 and 1 h^{-1} Mpc.

2.4. The nearest neighbor

For a given target galaxy with absolute magnitude M_r selected from a volume-limited sample its nearest neighbor is found in the following way. The closest neighbor is the galaxy brighter than $M_r + 0.5$ with the smallest projected separation across the line of sight from the target galaxy and with a radial velocity difference less than V_{\max} . In the case of D4 containing galaxies brighter than $M_r = -19.5$, we study only those target galaxies brighter than $M_r = -20.0$ so that their neighbors are complete. These criteria are empirically found from the sample. When we adopt galaxies fainter more than 0.5 magnitude as neighbors, our conclusions remain the same but our statistics become worse as the number of target galaxies becomes smaller. It also reflects the fact that the effects of the neighbor are more prominent when the neighbor is brighter than the target galaxy.

To determine V_{\max} we searched for all neighbor galaxies with velocity difference less than 1000 km s^{-1} with respect to each target galaxy and with magnitude not fainter more than 0.5. Figure 1 shows the velocity difference between the target galaxies with $M_r = -19.5 \sim -22.0$ and neighbor galaxies (in the D3 sample) brighter than $M_r = -19.0$ as a function of projected separation. Only the galaxies with measured redshifts are used. It was found that the RMS velocity difference of the neighbors is nearly constant out to the projected separation of $50 h^{-1}$ kpc, and is 255 and 169 km s^{-1} for early and late type target galaxies, respectively. We adopt $V_{\max} = 600$ and 400 km s^{-1} for the early and late type target galaxies. These limits correspond to about 2.3 times the RMS values.

3. RESULTS

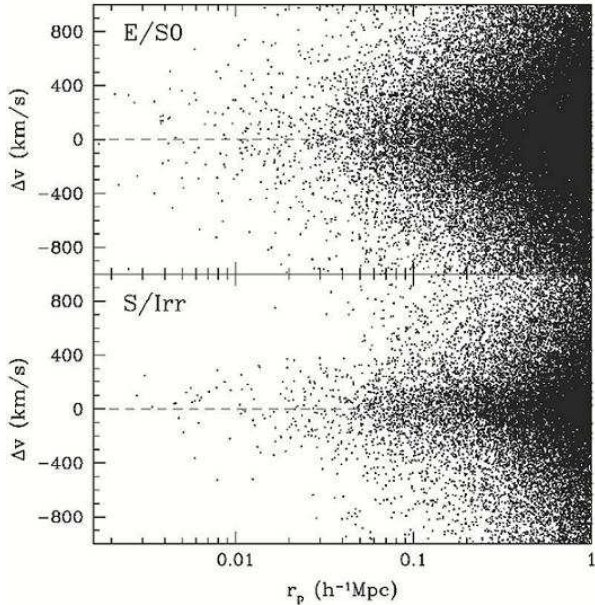


FIG. 1.— Velocity difference between the target galaxies with $-19.5 > M_r > -22.0$ and their neighbors brighter than $M_r + 0.5$ as a function of the projected separation. Most close neighbors have velocity difference less than 600 and 400 km s^{-1} when the target galaxy is an early (E/S0) and late (S/Irr) morphological type, respectively. The bottom panel for the late type galaxy indicates that contamination due the interlopers are serious when $\Delta v > 600 \text{ km s}^{-1}$.

3.1. Morphology Transformation

We first choose galaxies in the D4 sample with absolute magnitudes from $M_r = -20.0$ to -20.5 . They are basically L_* galaxies (see Table 2 of Paper I for the Schechter luminosity function parameters of the SDSS galaxies). The large-scale background environment is divided into high ($\rho_{20}/\bar{\rho} \geq 20$), medium ($3 \sim 20$), and low (≤ 3) cases. We then divide the small-scale neighbor environment into two cases when the closest neighbor is of early or late morphological type. Then we look at the morphology of the target galaxy as a function of the neighbor density ρ_n when its luminosity, background density, and neighbor morphology are all fixed. We first show Figure 2 for an intuitive understanding of the effects of the neighbor’s morphology and distance on the morphology of the target galaxy. At a fixed luminosity bin the probability of a galaxy to be an early type is a sensitive function of the projected separation of the neighbor. It also depends critically on the neighbor’s morphology at separations shorter than about $500 h^{-1} \text{ kpc}$. However, at larger separations the dependence of f_E on the neighbor morphology disappears.

To obtain a deeper physical understanding we now use the mass density due to the neighbor relative to the mean density of the universe as the abscissa of Figure 3. On the right side of the figure the upper three curves are the cases when the nearest neighbor is an early type and the lower two curves are for late type neighbor cases. The numbers next to the curves are the ranges of $\rho_{20}/\bar{\rho}$. It can be immediately noted that the galaxy morphology is still a very sensitive function of the environment determined by the nearest neighbor even if both luminosity and the large-scale density environment are fixed. According to the morphology–‘density’ relation (cf. Fig. 5

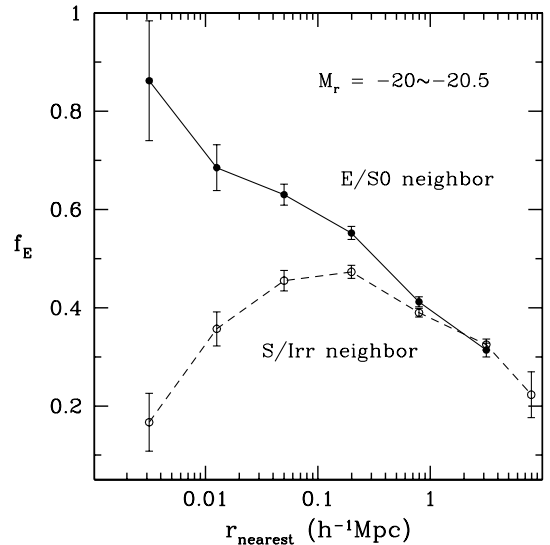


FIG. 2.— Fraction of early (E/S0) morphological type galaxies as a function of the distance to the nearest neighbor. The luminosity of the target galaxies is fixed to $M_r = -20.0 \sim -20.5$. The solid line with filled dots is the case when the nearest neighbors are early types, and the dashed line with open circles is for the late (S/Irr) type neighbor cases.

of Park et al. 2007) galaxies are mostly of late type at very low (large-scale) densities and of early type at very high densities. However, Figure 3 tells that the majority of galaxies are of early type even at low densities if they have close early type neighbors, and that the majority of galaxies are of late type even at high densities if they are very isolated from other galaxies of comparable or brighter luminosity. Figure 3 tells us more facts. When $\rho_n/\bar{\rho} \leq 10^2$, the probability f_E for a galaxy to be an early type does not depend on the neighbor’s morphology. Its dependence on ρ_{20} is also weak (but discernable). It is only the neighbor density ρ_n (besides luminosity) which significantly affects f_E ; the probability monotonically increases as ρ_n increases. Hydrodynamic or radiative effects of the neighbor are not likely to be responsible for this increase because there is no neighbor morphology dependence. The effects acting in the environments like cluster or group can not be responsible for the increase of early type fraction because the dependence on the large-scale background is insignificant in this range of ρ_n . A possible mechanism responsible for this is the tidal effects by the neighbor because the net effects of tide depend only on kinematic quantities such as separation, mass, size, and relative velocity (eq. 5). Tidal effects can accelerate the consumption of the cold gas in galaxies and tend to transform late types into early types.

It will be interesting to quantitatively estimate the strength of the tidal effects generated by a neighbor located at about the virial radius. Consider a galaxy having mass M_0 within radius R_0 . Its gravitational binding energy is $E_b \approx GM_0^2/R_0$. The tidal energy deposit by a neighbor galaxy with mass M_n and relative velocity Δv_n is given by equation (5) times M_0 . When the separation between the galaxies is much larger than the RMS radius of the galaxy, the tidal energy deposit relative to the binding energy is given by

$$\Delta E/E_b \approx GM_n^2 a^2 R_0 / M_0 \Delta v_n^2 r_p^4. \quad (6)$$

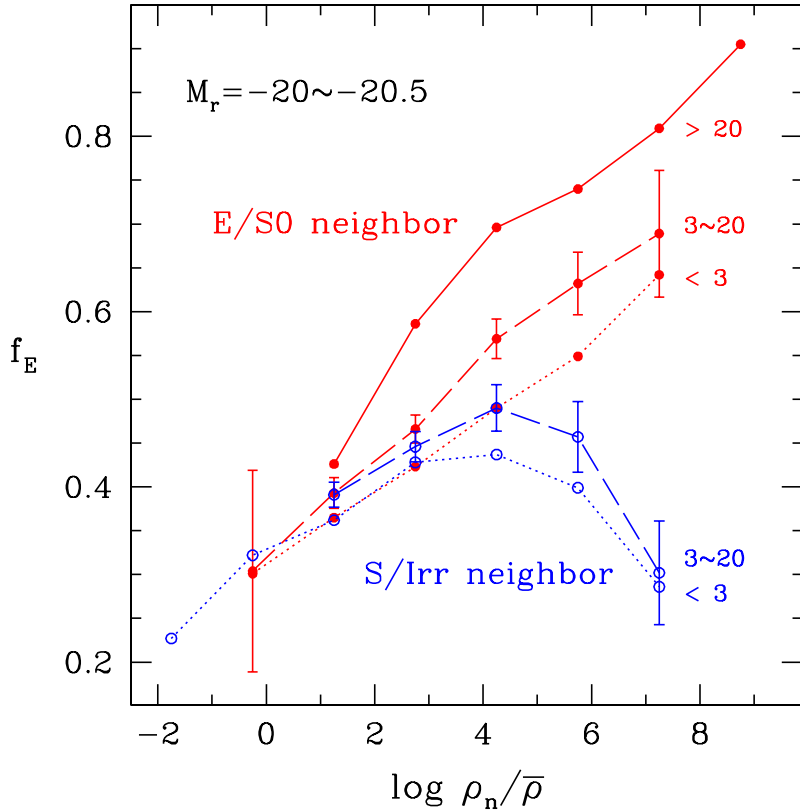


FIG. 3.— Fraction of early (E/S0) type galaxies as a function of the small-scale density due to the nearest neighbor. The luminosity of the target galaxies is fixed to $M_r = -20.0 \sim -20.5$. Each curve represents the case of a fixed large-scale background density estimated by using 20 nearest galaxies brighter than $M_r = -19.5$. The range in $\rho_{20}/\bar{\rho}$ is labeled at the right of each curve. The upper three curves are the cases when the nearest neighbor is an early type galaxy, and the lower two cases are when the nearest neighbor is a late (S/Irr) type.

If we adopt $M_0 = M_n = 1 \times 10^{12} h^{-1} M_\odot$, $r_p = R_0 = 2a = 300 h^{-1}$ kpc, and $\Delta v_n = 100$ km/s, we obtain $\Delta E/E_b = 0.36$. Therefore, the tidal effects between the dark halos of equal mass galaxies is not negligible at the separation of about the virial radius (see below). But the tidal force of the neighboring galaxy probably do little directly to the stellar and gas components of the galaxy because of small a and R_0 for these components. It remains to examine if the rearrangement of the dark matter in the halo during the distant encounter can perturb the embedded late type galaxy significantly enough to accelerate the consumption of its cold gas.

When $\rho_n/\bar{\rho} \geq 10^3$, however, the probability at a fixed luminosity depends on all parameters, ρ_n , ρ_{20} , and neighbor's morphology, in a complicated but understandable way. When galaxies have a late type closest neighbor, their $f_E(\rho_n)$ deviates from that of the galaxies with early type neighbors at $\rho_n/\bar{\rho} \approx 10^3$, and starts to drop at $\rho_n/\bar{\rho} \geq 10^4$.

It is very important to note that this transition happens at the virial density. The virialized density is $\rho_{\text{virial}}/\bar{\rho} = 18\pi^2/\Omega_m(H_0 t_0)^2 = 766$ relative to the mean density in the model universe we adopted (Gott & Rees 1975). Then equations (3) and (4) give the radius of the virialized region $r_p \approx 240$ and $300 h^{-1}$ kpc for the late and early type galaxies with $M_r = -20$, respectively. The neighbor galaxy is holding both cold and hot gases within the virial radius, and they can affect the fate of the galaxy falling into the region. If the neighbor is a late type galaxy, it is possible for its cold gas to flow into

a trapped early type galaxy and transform it to a late type. If this picture is true, then one would expect to find galaxies which appear to indicate hydrodynamic and/or radiative interactions between close pairs of galaxies before or without merger. Figure 4 shows a few examples. A $20 h^{-1}$ kpc scale bar at the rest frame is given to each panel. The late type galaxies in the panels from (a) to (e) seem to be transferring cold gas to their early type companions.

In panel (a) a long bridge extending from one spiral arm of a late type galaxy ($z = 0.0395$) is connected to an early type galaxy ($z = 0.0397$). Despite its morphology the early type galaxy is very blue ($u - r = 1.73$), and has extremely strong emission lines indicating active star formation. The shape of this system has a surprising resemblance with a simulation made by Cullen et al. (2007). They presented the observed spatial and kinematic distribution of the atomic (HI) and molecular (CO) gases in the spiral-elliptical interacting pair, Arp 104. They also made a series of N-body simulations of the encounter between a spiral and an elliptical galaxy to reproduce a system such as Arp 104. Figure 8 of their paper is a best fitting case. However, we note that the mass distribution in their simulation result looks even closer to the system in panel (a). An important lesson from their simulation is that a fraction of mass in the disc of the late-type galaxy can be transferred to the early-type component, and the spiral galaxy in panel (a) is probably feeding its disk material to its elliptical neighbor, which can be responsible for its spectral characteristics.

The panel (b) might be showing an example of the early-to-late transformation. The galaxy VCC1748 (Binggeli, Sandage, & Tammann 1985) with the recession velocity of 11308 km s^{-1} is at the lower right from the center. It seems to be originally a red elliptical galaxy, but is now feathered with two blue spiral-looking arms. Along the direction of its major axis is a blue spiral galaxy VCC1752 having almost the same recession velocity of 11299 km s^{-1} . The separation of two galaxies is only $34.5 h^{-1} \text{ kpc}$, and the local density felt by VCC1748 due to VCC1752 is 3.5×10^5 relative to the mean density, much higher than the virial density. One arm of the spiral galaxy is clearly connected to VCC1748 suggesting that the two arms are formed by the cold material flowed from VCC1752 along the bridge. VCC1748 has previously been classified as SBa, and seems to be an example that an elliptical galaxy transforms into a spiral when it closely encounters a gas-rich spiral without or before a merger event. The systems from panels (c) to (e) also indicate mass transfer from a late type galaxy to an early type.

In fact, the mass transfer between galaxies during interactions has been widely studied both observationally and by numerical simulations. Simulations indicate that the detailed interaction features and the total mass transferred depend critically on the interaction parameters (Toomre & Toomre 1972; Sotnikova 1990; Mihos & Hernquist 1994). In particular, Walin & Stuart (1992) pointed out that the transfer of gas between galaxies can occur after they pass the point of perigalacticon. Observational evidence for mass transfer between galaxies has long been suggested by many studies. Knapp, Turner, & Cunniffe (1985) examined the HI content of elliptical galaxies and suggested that the gas has an external origin. Counterrotating disks or bulges in spirals and ellipticals with dust lanes can be interpreted as results of gas flows from the outside (Bertola et al. 1998; Prada et al. 1996). Many examples of ongoing mass transfer between interacting galaxies have been studied. Some of them are Arp 105 (Duc et al. 1997), Arp 194 (Marziani et al. 2003), NGC 1409/1410 (Kell 2004), and Arp 104 (Cullen et al. 2007).

The top three curves of Figure 3 indicate that when the nearest neighbor is an early type, f_E keeps increasing as ρ_n increases above the virial density. In the light of the previous interpretation this would be because the early type neighbor has a negligible amount of cold gas and both its hot gas and tidal effects tend to make the target galaxy falling within its virial radius an early type. It is well-known that early type galaxies have extended X-ray halos (Ellis & O’sullivan 2006). The X-ray emission and the hydrodynamic effects of hot gas can only accelerate consumption of cold gas in the close neighbor. Since the bifurcation of f_E for the late and early type neighbors occurs nearly at the virial density of the neighbor, the hydrodynamic effects seem more responsible for the morphology transformation than the radiative effects which should be less sensitive to a particular scale. This may not be true for galaxies much fainter than $M_r = -20$, and the ionizing radiation from a bright elliptical galaxy could affect the cold gas content of faint spirals beyond the virial radius. This seems to happen at least to the satellites of bright early and late type galaxies (Ahn, Park, & Choi 2007).

The early type galaxies in panel (f) of Figure 4 support

the argument that the hot gas of an early type galaxy can remove cold gas from its neighbor (in this case we have redshift only for the middle one. We assume the two early type galaxies form a real interacting system. They have nearly the same photometric redshifts). The galaxy in the middle has a blue arc on the side facing the spiral galaxy. However, the galaxy does not have such an arc on the opposite side facing brighter elliptical galaxy. We speculate that the hot gas of the elliptical neighbor at the bottom may be responsible for non-existence of the second arc of the middle galaxy as an elliptical neighbor can ionize or push away the cold gas of its neighbor galaxy by a direct physical contact and make it look like an early type (see Sofue 1994 for a demonstration of such process in simulations). We conclude that the physical properties of close neighbors are of paramount importance in the fate of a galaxy.

One can also learn from Figure 3 that f_E is systematically higher for higher ρ_{20} when ρ_n is higher than the virial density. The mechanisms suggested for morphology transformation to early type due to large-scale environment include the ram pressure stripping of a late type galaxy falling into a cluster holding hot gas (Gunn & Gott 1972), removal of hot gas reservoir and stopping of cold gas supply (strangulation; Larson et al. 1980), or impulsive heating due to numerous encounters with other galaxies in high density environment (harassment; Moore et al. 1996). Even though these mechanisms may be acting in the very high large-scale density regions, none of these can be fully responsible for the large-scale background dependence we found because they all predict that f_E is enhanced as ρ_{20} increases independently of ρ_n , which contradicts Figure 3. (Note also that we cannot resolve the virialized region in the large-scale density ρ_{20} .) The fact that the strong ρ_{20} dependence is observed only when $\rho_n > \rho_{\text{virial}}$, suggests that the effect of the background is indirect, and the mechanism may be associated with a physical property of the closest neighbor which in turn depends on the large-scale environment. For example, this dependence can arise if the density and temperature of the hot gas held by galaxies are higher in higher density environments. Such a trend has been found only for the brightest group or cluster elliptical galaxies. They are reported to have higher X-ray luminosity at given optical luminosity in higher density regions (O’sullivan et al. 2001).

Since it is very important to know the dependence of the X-ray emitting hot gas of normal early type galaxies on the large-scale environment to understand the dependence of f_E on ρ_{20} , we investigated the relation between X-ray luminosity of early types and the large-scale background density. We used X-ray data from the *ROSAT* All-Sky Survey (Voges et al. 1999) positionally matched with galaxies in the SDSS DR4plus catalog. Among the matched sources there are 78 early types brighter than $M_r = -19.5$ within the volume of D4 sample, we find that there exists a clear positive correlation between the X-ray luminosity and ρ_{20} at fixed optical (*r*-band) luminosity. Our accurate density estimator enabled us to detect this correlation. The dependence of f_E on ρ_{20} at $\rho_n > \rho_{\text{virial}}$ can be explained by this correlation. The dependence is indirect and becomes effective only when the hot gas of the neighbor galaxy starts to be influential at separations between galaxies less than the virial radius.

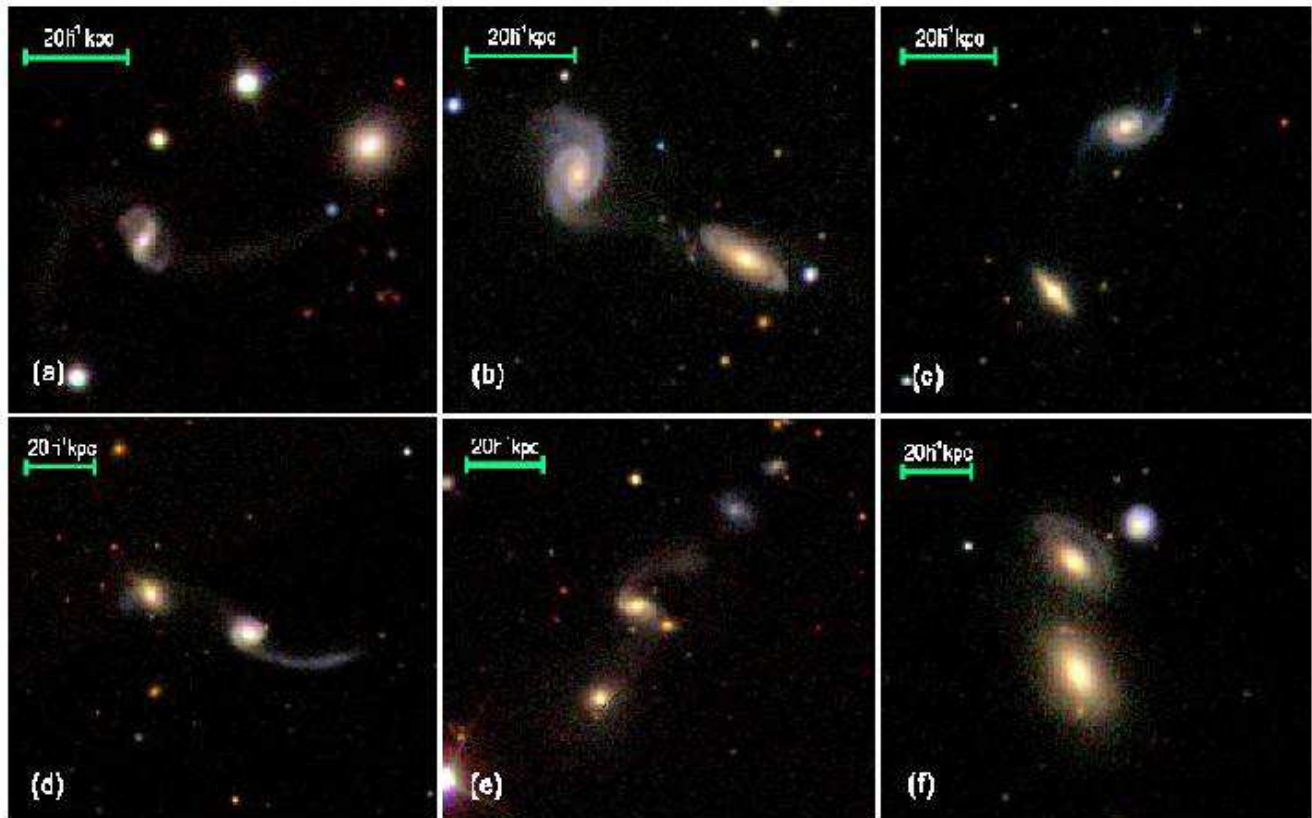


FIG. 4.— (a) - (e): Examples of interacting galaxies suggesting gas transfer from a late-type galaxy to an early-type galaxy without or before merger. The red galaxy with two blue spiral arms, VCC1748, in panel (b) might be a case showing the morphology transformation from early to late type. (f): An example suggesting that a bright early-type galaxy affect the cold gas of a neighboring galaxy. The blue arc of the middle galaxy is not seen at the side facing the bright elliptical galaxy below. The position (RA, DEC) of the late type galaxy in each panel is (189.5657, 7.8204), (181.6186, 63.6299), (174.8445, 64.8037), (235.4750, 29.9913), (128.5264, 46.4387), and (166.6741, 42.8220), from panel (a) to (f), respectively.

So far, our study is done for the case when the luminosity of the target galaxies is restricted to $M_r = -20.0 \sim -20.5$. Figure 5 shows how the morphology transformation relation scales with luminosity. The bottom two (dotted) curves are the same as those in Figure 3 but summed over all large-scale background densities. The early-type fraction f_E monotonically increases as ρ_n increases when the neighbor is an early type, but drops at $\rho_n/\bar{\rho} > 10^4$ when the neighbor is a late type. The remaining curves are obtained from a deeper and brighter volume-limited sample of galaxies with $M_r < -20.0$ (Sample D5 in Paper I). The middle two curves are for galaxies with $-20.5 \geq M_r \geq -21.0$ having an early (higher f_E at high ρ_n) or late-type closest neighbor. The top two curves are for the half magnitude brighter galaxies with $-21.0 \geq M_r \geq -21.5$. We first note that the bifurcation of the early and late type neighbor branches occurs at the same $\rho_n/\bar{\rho} \approx 10^3$. The neighbor's morphology is still an important environmental factor in the morphology transformation at these brighter magnitudes. Figure 5 tells that the whole morphology transformation relations as a function of ρ_n and neighbor's morphology, scale monotonically with luminosity. We have also confirmed this scaling at the fainter magnitude range from $M_r = -19.5$ to -20.0 . Above $M_r = -21.5$ a similar scaling is seen but the scaling amplitude is suddenly very large. This is because the fraction of early type galaxies increases steeply above the magnitude of

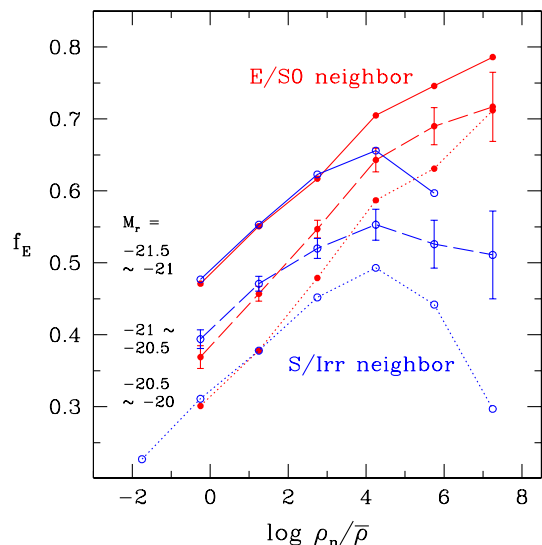


FIG. 5.— Scaling of the morphology–neighbor density relation as a function of target galaxy luminosity. Bottom two dotted curves used galaxies in D4 sample with M_r from -20.0 to -20.5 , and having early (filled circles) and late (open circles) neighbors. The upper four curves used D5 sample.

$M_r \approx -21.3$ (See Fig. 8 of Paper I). They are often the central galaxies in groups and clusters.

To summarize, a late type galaxy tends to become an

early type due to the tide exerted by its closest neighbor when it is separated by more than the virial radius of the neighbor. At separations less than the virial radius the galaxy still tends to transform to an early type if the neighbor is an early type. This trend is accentuated at higher large-scale background density. But if the neighbor is a late type, the direction of morphology transformation tends to reverse and an early type can become a late type as it approaches its bright spiral neighbor. When one considers galaxies of different luminosity, all behaviour remain the same and the probability for a galaxy to be an early type simply scales with luminosity over the absolute magnitude ranges we study. Therefore, our understanding of galaxy morphology can not be complete unless we understand how this luminosity–morphology relation originates.

3.2. Luminosity Transformation

From Figure 3 we were able to propose a number of physical processes playing roles in the galaxy morphology transformation. However, one thing that Figure 3 can not tell us is what happens when galaxies (located at very high ρ_n) finally merge. After a galaxy undergoes a major merger with its closest neighbor, the next closest one will become the new closest neighbor. The luminosity or mass of the merger product will be higher than those of the merging galaxies, and the small-scale density ρ_n will drop greatly as the next closest neighbor as bright as the merger product will be usually far away. If the galaxies had cold gas, the star formation must become relatively higher during the merger and the total cold gas content in the merged one will be less than the sum of the cold gas before the merger due to merger-induced starbursts. The next major merger will occur with a more massive galaxy (as massive as the merged product) which tends to have a lower fractional mass of cold gas. As this approach-merge process repeats, the fractional mass of the merger product in the form of cold gas will eventually vanish.

This scenario can explain why almost all most massive galaxies are early types. The scenario can be supported by our finding that galaxy luminosity depends on ρ_n at a fixed large scale density. When one inspects the effects of ρ_n or the nearest neighbor distance on various physical parameters of galaxies, one finds only a very weak signal for all parameters except for luminosity (Y.-Y. Choi et al. 2007, in preparation). Figure 6 shows the absolute magnitudes of galaxies in *D4* as a function of ρ_n . The upper panel is for early type galaxies, and the bottom panel is for late types. As in Figure 3, we divide the large-scale background mass densities of galaxies into three bins according to their ρ_{20} . We plot only those galaxies sitting at the highest ρ_{20} (red dots) or at the lowest ρ_{20} (blue dots) bins to avoid overcrowding. Three curves are the median magnitudes of galaxies in three ρ_{20} bins as a function of ρ_n , and the curves for early types are repeated in the bottom panel as dashed curves.

One can immediately notice that the luminosity of galaxies brighter than $M_r = -20$ and located in high ρ_{20} regions is much higher at smaller ρ_n . Namely, galaxies are brighter as they are more isolated. And it is a strong function of ρ_n when $\rho_n/\bar{\rho} < 10^2$. But it can be also noticed that luminosity is nearly independent of both ρ_n and ρ_{20} when $\rho_n/\bar{\rho} > 10^3$, and that all these behaviours are almost the same for both early and late

type galaxies (but early types are slightly brighter than the late types in the magnitude range we explore). We find the same behaviour of luminosity when fainter galaxies ($M_r \leq -19.5$) are included. To explain why isolated galaxies are brighter in high ρ_{20} regions and become faint as ρ_n increases, one can argue that brighter galaxies preferentially form in higher large-scale density regions and that galaxies become fainter by tidal stripping as they approach each other. However, this scenario is contradictory with the fact that the median luminosity is almost the same in different ρ_{20} regions at $\rho_n/\bar{\rho} > 10^3$, and that galaxy luminosity is independent of ρ_n at very high ρ_n where the tidal stripping should be more active.

An important fact that should be noted in Figure 6 is that galaxies become more isolated (small ρ_n) when ρ_{20} is smaller or when luminosity is higher. In high ρ_{20} regions galaxies are on average much closer (higher ρ_n) to one another than those in low ρ_{20} regions. Inevitably, the merge rate is relatively higher in higher ρ_{20} regions. We have visually identified merging (or close encounter) galaxies in the *D2* sample brighter than $M_r = -20$. We looked for strongly interacting galaxies that show distorted bodies with connecting bridges and/or trails, and have magnitude difference less than 1.5. We included the cases that an early type galaxy is seen within the optical image of the other early type. We found, in the three density bins of $\rho_{20} < 3$, $3 \sim 20$, and > 20 , the fractions of galaxies undergoing major merger/interaction are 3.0, 4.8, and 6.8 %, respectively. This confirms the strong dependence of the major merger/interaction rate on ρ_{20} (D. G. Kim et al. 2007, in preparation). The galaxy merger rate in high density regions must be higher than our estimate because there are more early type galaxies at high densities and the merge between early types is more difficult to notice as merging early types are less likely to show bridges or trails than late types. When a galaxy merges with another of equal mass, the merger product will have twice the mass if the mass loss during the merger is negligible. Since galaxies with twice the mass of the merging galaxies will be rarer, it will be more difficult for the merger product to find a neighbor that can significantly influence its morphology and luminosity. Therefore, the merger product will jump to the upper (brighter) left (low ρ_n) part of each panel in Figure 6, as we argued before. The rapid brightening of galaxies at $\rho_n/\bar{\rho} \leq 10^2$ in the case of the highest ρ_{20} bin, may be due to this process. At what value of ρ_n will the galaxy find itself after merger? It is reasonable to predict that the new ρ_n is typically less than ρ_{virial} . If new $\rho_n > \rho_{\text{virial}}$, it implies two merging galaxies were already within a virial radius of a third one of about twice mass before merger. This is not very likely because the more massive one in general impedes their merger by tidal force and tends to swallow the little ones before they merge unless the pair were already ready to merge before it fell into the more massive one. This can explain why luminosity is nearly constant for galaxies at $\rho_n > \rho_{\text{virial}}$. Recently-merged galaxies usually do not fall at such ρ_n . Therefore, the merger hypothesis can explain all features of Figure 5.

To find more dynamical evidence for this scenario we inspected the late type galaxies showing indications of recent merger events. Our prediction is that there are more galaxies showing post merger features at $\rho_n < \rho_{\text{virial}}$ for a given luminosity and a fixed large scale density.

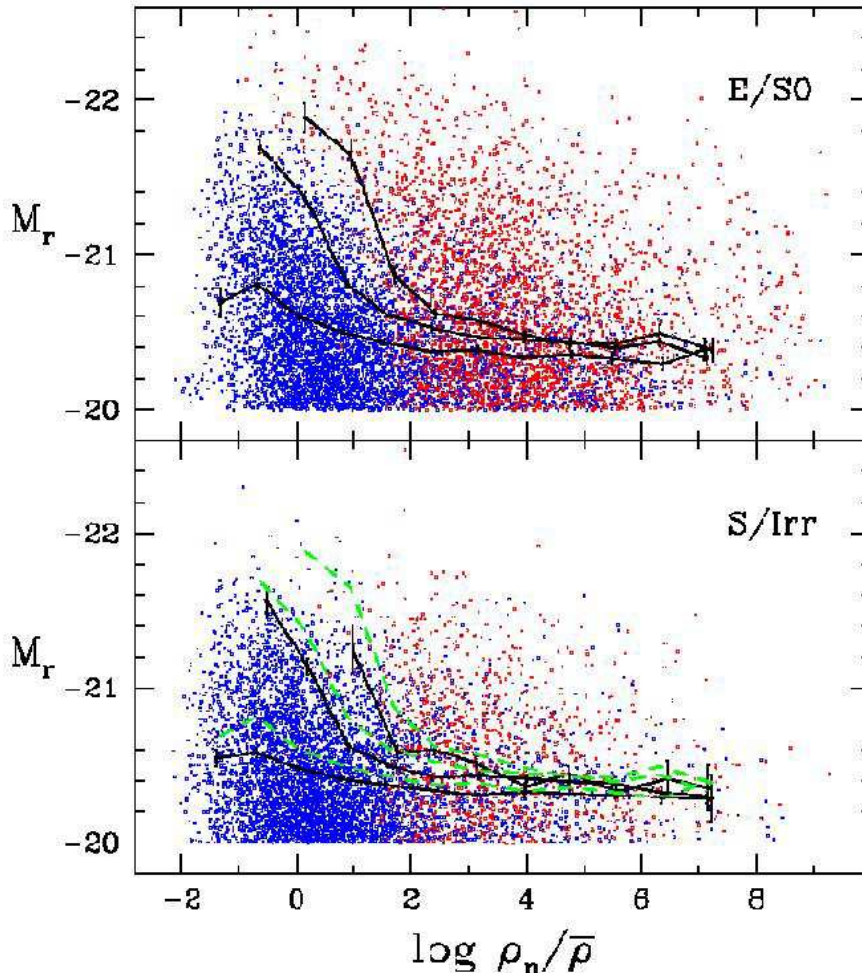


FIG. 6.— The absolute magnitude of galaxies as a function of the neighbor density ρ_n . The upper panel shows early (E/S0) type galaxies and the lower panel is for late (S/Irr) types. Red dots are for galaxies located at $\rho_{20}/\bar{\rho} \geq 20$, and blue dots are for < 3 . The top, middle, and bottom curves are the median magnitudes of galaxies located at $\rho_{20}/\bar{\rho} \geq 20$, $3 \sim 20$, and < 3 , respectively. Three curves for early types are repeated in the bottom panel as dashed curves.

For late type galaxies we define post merger features as large displacement of the galaxy nucleus from the center, turmoil features, and/or very close double cores. The selection is subjective, but is made only for quite clear cases. Only late types are used for higher reliability. For galaxies with $M_r = -20.0 \sim -20.8$ and located in the highest large-scale background density region ($\rho_{20}/\bar{\rho} > 20$) the fractions of galaxies showing the post merger features are 3.3 and 3.1% when $\rho_n/\bar{\rho} < 766$ and $766 \leq \rho_n/\bar{\rho} < 10^4$, respectively. For more luminous galaxies with $M_r = -20.8 \sim -21.6$ the fractions increase to 10.8 and 4.0 %, respectively. Therefore, there are more recently merged galaxies among isolated ones than among those with close neighbors.

Figure 7 illustrates a merger in an isolated environment. The r -band magnitude and redshift are given to all galaxies brighter than $r = 17.6$. At the center of the picture is a spiral galaxy NGC3695 with two cores indicating that it is at the ending stage of merger. NGC3695 has $M_r = -21.27$, and is a blue spiral galaxy showing very strong star formation activity. Nearly equal brightness of the two nuclei implies that two galaxies of comparable mass have merged. Since NGC3695 is completing merger, the next closest galaxy will become a new neighbor.

The bright galaxy at the lower left of the picture is NGC3700. Because NGC3700 has velocity difference of $12,300 \text{ km s}^{-1}$, it does not qualify as a neighbor. The closest neighbor is found at the separation of $1h^{-1} \text{ Mpc}$, and NGC3695 is a good example of very isolated galaxy which once was a close pair of galaxies.

To summarize, galaxies travel from the left to the right of Figure 6 at a given luminosity. During this travel, galaxies are affected by the morphology transformation processes suggested by Figure 3, and can jump from one panel to the other. When they reach very high ρ_n , they undergo a merger and become brighter. As they become brighter through mergers, they will find themselves more isolated from their neighbors of comparable mass. As galaxies repeat such travel, the fractional mass in cold gas will decrease and galaxies with higher mass will tend to be of early type.

4. DISCUSSION

A full understanding of the origin of galaxy morphology will be obtained if one finds the initial distribution of morphology and the rule of morphology transformation. The present study addresses the second issue. If galaxies transform their morphology and luminosity in accordance with the unified scenario we propose, a number

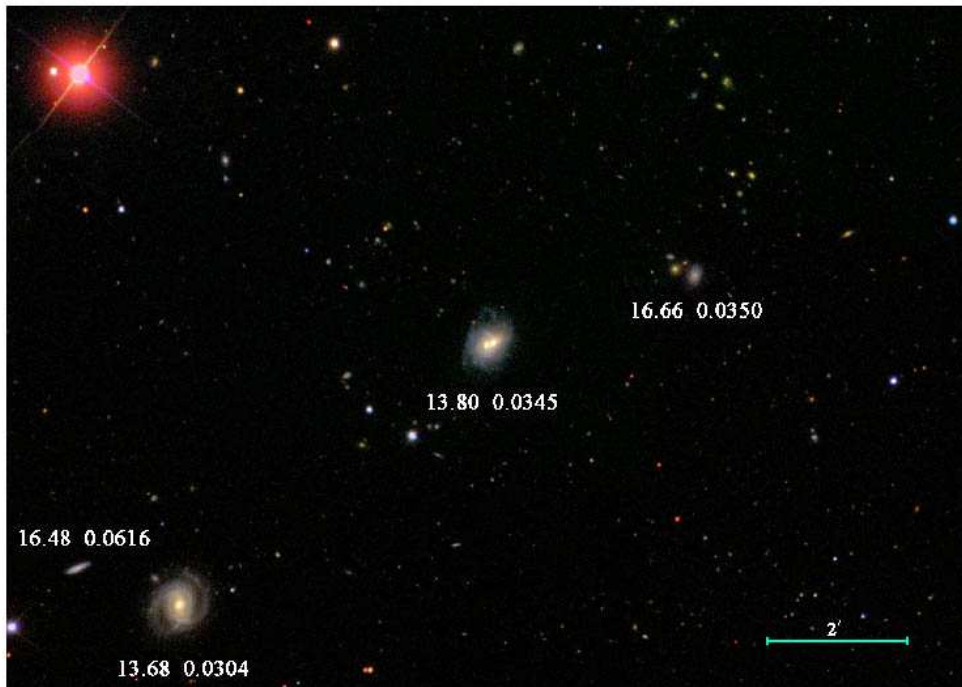


FIG. 7.— An example of the isolated galaxy which once was a close pair of galaxies. At the center is a spiral galaxy NGC3695 which has two cores, indicating that it is a recent merger product. Its closest neighbor is located at the separation of $1h^{-1}$ Mpc (not seen in this picture). At the lower left is another spiral galaxy NGC 3700, which is a foreground object not directly interacting with NGC3695. The r -band magnitude and redshift are given to galaxies brighter than $r = 17.6$.

of galactic phenomena found in the past can be qualitatively explained. Because the merger rate is higher in the higher large-scale density regions, there are more bright merged galaxies in high density regions, which can explain the luminosity-density relation (Paper II). As the merger process repeats, galaxies become brighter but also tend to become early types because the cold gas fraction decreases. This can explain the luminosity-morphology relation. Furthermore, the effect of hot gas of the neighbor on a galaxy orbiting within the virial radius tends to make the galaxy an early type and its effects are stronger in high large-scale density regions. This can explain the morphology-density or morphology-(clustercentric) radius relation (more discussion is given below).

In addition to these important relations our picture can explain the following.

1. *Holmberg effect* Holmberg (1958) discovered that the color of paired galaxies are closely correlated. We predict that as two galaxies approach each other and enter into the virial radius, hydrodynamic and radiative interactions of cold and hot gases occurs. The primary galaxy tends to make the pair system have common properties. The color of the secondary can become closer to that of the primary.
2. *Star formation rate-density correlation* The fraction of star-forming galaxies is known to depend strongly on the local density. Balogh et al. (2004a) showed that the fraction of $H\alpha$ emission-line galaxies is lower in regions that are overdense at both 3.85 and $0.77h^{-1}$ Mpc scales. To a large extent this correlation is associated with the morphology

density relation. Our picture predicts that the cold gas content and thus the SFR in galaxies will be lower in higher large-scale density regions where the merger rate is higher and the early-type fraction is higher. At the same time, the morphology of a galaxy is sensitive to that of its neighbor when it is located within the virial radius of the neighbor. The SFR must be so too. The neighbor's morphology depends on the background density when the pair separation bin is small than the virial radius. Therefore, the SFR should appear dependent on both small and large-scale densities. When the large-scale density and neighbor morphology are fixed, the SFR of galaxies in close pairs is predicted to be depressed for the early type neighbor case or enhanced for late type neighbor case.

3. *Conformity in galaxy morphology type* This is essentially the same as the previous two relations. It has been observed both in group/cluster environment and at galaxy scales. Weinmann et al. (2006) reported that a late-type central galaxy has a significantly higher fraction of late type galaxies within its halo than an early-type central galaxy of the same mass (see also Hickson et al. 1984 and Ramella et al. 1987). This can be just because of the strong hydrodynamic and radiative influences of the bright central galaxy on the less bright surrounding galaxies which are orbiting within the virial radius of the central one. This galaxy morphology conformity is also observed within the halos of individual galaxies. An elliptical galaxy is found to host a swarm of early type satellite galaxies while a gas-rich spiral galaxy tends to hold many

late type satellites (H. Ahn et al. 2007 in preparation). This is a scaled-down version of the phenomena observed in groups and clusters, and can be consistently explained by our picture.

4. *Morphology–density versus morphology–radius relation* Galaxy morphology depends strongly on the clustercentric radius (Melnick & Sargent 1977) or local density of galaxies in clusters (Dressler 1980). It would seem impossible to find which of the factors is the more fundamental. Our picture claims that it is the local density which really controls the phenomena. The large-scale background density determines the average distance to the nearest neighbor and the merger rate which in turn determines the mean brightness and morphology of the neighbor. The small-scale density due to the nearest neighbor determines the strength of the tidal and hydrodynamic effects. The virial radii of the group/cluster a galaxy belongs to, or of its neighbor galaxy are statistically determined by local densities. When a galaxy enters within the virial radius of the group/cluster or of the neighbor galaxy, it starts to interact with the hot/cold gas trapped within the radius. Therefore, the virial radius has a fundamental importance in the evolution of galaxy morphology.
5. *Morphology-dependent large-scale clustering* It is well-known that the spatial distribution of the early-type galaxies has higher clustering amplitude than the late types. This can be because the early types preferentially form in high density regions and their clustering is more biased than the late types relative to the mass. However, our results imply that even if the initial morphology of the newly-born galaxies is of late type, the luminous early type galaxies are formed preferentially in high density regions because the binary interaction is more frequent, the merger rate is higher, and the cold gas consumption is faster there. Once the early type galaxies with hot gas appear in high density regions, they will promote the transformation of morphology of neighboring spirals through galaxy-galaxy interaction. Since high density regions are compact, this will result in the morphology-dependent clustering amplitude.

Our picture on the transformation of galaxy morphology and luminosity also explains some recent findings and can make predictions on galaxy properties.

1. *Existence of early types in underdense regions* In our picture early type galaxies can form in low density regions as well as in high density regions but at a lower efficiency through infrequent pair interactions and mergers. It can be inferred from Figure 6 which shows there are much fewer galaxies with $\rho_n/\bar{\rho} > 10^3$ in low density regions (blue points). It predicts that, in underdense regions where there are more gas-rich late-type neighbors, the very bright early types will be very rare and the fraction of blue star-forming early types will be higher. This is exactly what is seen in Figure 11 and 12 of Paper

II. There are ‘normal’ ellipticals even in very underdense regions as demonstrated by the fact that the red-sequence of early types hardly changes as the large-scale density changes. However, in underdense regions the red-sequence has a much shorter extension toward the bright magnitudes and the fraction of blue galaxies increases. The fractions of early-type galaxies brighter than $M_r = -21.5$ among those with $M_r < -19.5$ are 9.4, 6.6, and 2.8 % in the regions where $\rho_{20}/\bar{\rho} \geq 20$, $3 \sim 20$, and < 3 , respectively. On the other hand, the fractions of blue early type galaxies with $u - r < 2.3$ and $M_r \leq -19.5$ are 1.2, 2.3, and 3.4 % in those three regions. Properties of early type galaxies in low density regions are also studied by Croton et al. (2005) and Rojas et al. (2005). The simple scenario that postulates formation of all early type galaxies in initially high density regions has a difficulty in explaining existence of the normal and blue ellipticals in very low density regions.

2. *Isolated galaxies* Isolated galaxies are often studied in the hope that the evolution of galaxies can be understood with no contamination from environment-related processes. Isolated galaxies are usually defined as those which do not have companions brighter than a certain magnitude difference within a certain projected distance and radial velocity difference. They are considered to be passively evolving galaxies formed in isolation via gravitational collapse of a primordial protogalactic cloud (Marcum, Aars, & Fanelli 2004). However, our scenario drawn from Figure 6 predicts the most isolated galaxies are likely to be those that experienced a major merger relatively recently and whose internal evolution was greatly disturbed. This is particularly so in high density regions or for very bright galaxies. The wish for freedom from environmental effects will be approximately fulfilled only for the galaxies isolated at very low densities, namely for the void galaxies. For example, Marcum et al. (2004) have selected extremely isolated elliptical galaxies from the Catalog of Isolated Galaxies (Karachentseva 1973) and found that four out of nine showed merger signatures. It should also be noted that isolation of a galaxy is strongly correlated with the large-scale density and characteristics of isolated systems can be easily confused with those of underdense environment (i.e. Varela et al. 2004).
3. *Redshift evolution of morphology and luminosity* Our scenario is consistent with the common wisdom that galaxies were on average less massive in the past and that the late-type fraction of galaxy morphology was higher at higher redshifts. It predicts that galaxies located in high density regions should show relatively large differences in luminosity, color, SFR, and morphology as redshift changes because the mean separation between galaxies is smaller and the merger rate is higher there. The fraction of early type galaxies should monotonically decrease and the fraction of blue early type among early types should increase at higher red-

shifts. However, the energetic radiation from numerous active galaxies, which are a minor population in our sample, might have critical roles in the evolution at high redshifts. Much less evolution will be observed for galaxies in low density regions where the mean galaxy separation is large because the interaction between galaxies is weaker and merger is less likely. Correspondingly, the star formation–density relation will change in such a way that the strongest SFR of galaxies be observed in higher density regions as redshift increases (see Elbaz et al. 2007 for an observational detection of this phenomenon). Our scenario is also consistent with the recent finding from a N-body simulation that internal physical properties and spatial clustering of dark halos depend not only on the mass but also on the assembly history (Gao, Springel, & White 2005; Wechsler et al. 2006; Gao & White 2007; Croton, Gao, & White 2007). At high redshifts, galaxies at high densities are expected to be less depleted in cold gas and experience more frequent interactions than those at low densities. Since at higher redshifts the space was compressed but there were fewer number of massive galaxies, the merger rate of objects above a given mass is expected to evolve rather slowly (see Lotz et al. 2006 and Bell et al. 2006 for observational evidence)

The galaxy morphology can also evolve due to the infalling gas in the form of intergalactic medium or dwarf galaxies. In less massive halo, the disk can be formed by cold flows ($\sim 10^{4-5}\text{K}$), and in more massive halos the infalling gas is first heated by shocks to near the virial temperature ($\sim 10^6\text{K}$) before it is accreted to form a disk (Dekel & Birnboim 2006; Keres et al. 2005). The relative importance between the galaxy-galaxy interaction and the gas/dwarf accretion on morphology transformation will depend on the large-scale environment and the time scales of gas cooling and interaction between galaxies. For examples, the importance of the infalling gas will be relatively higher in low density regions where the interaction rate is lower and there are more gas rich faint objects. It is also possible for galaxies to transform their morphology between early and late types through secular internal processes like exhaustion of cold gas and aging of the stellar population. The time scale of such secular evolution is probably longer than those of galaxy interaction or gas accretion before the present epoch. It will be interesting to compare the relative importance of all these processes in different environments.

5. CONCLUSIONS

We have analyzed a set of volume-limited samples drawn from the SDSS data in order to understand the morphology–luminosity–environment relation. Our previous study on the environmental dependence of galaxy properties (Paper II) showed that most of the environmental dependence of physical parameters disappears once luminosity and morphology are fixed and that the morphological type of galaxies is affected by both small-scale (due to the nearest neighbor) and large-scale densities. In particular, a strong dependence of morphology on the nearest neighbor distance was discovered when the distance was about $200h^{-1}$ kpc. For galaxies with

$M_r = -19.0$, which is the faint limit of the sample D2 used in Paper II, the critical distance of $200h^{-1}\text{kpc}$ corresponds to the neighbor density of $\rho_n/\bar{\rho} = 520$ or 1040 for late or early type neighbor, respectively. This essentially corresponds to the virial density. In the present work, based on the lessons from the previous study, we divided the environment into the large-scale background density, small-scale density due to the nearest neighbor, and the nearest neighbor’s morphology. Our major findings are the following.

1. Transformation of galaxy luminosity and morphology classes is going on in all large-scale density environments through interactions and mergers between close galaxy pairs.
2. At galaxy pair separations larger than the virial radius of the neighbor galaxy, the morphological type of a galaxy is nearly independent of the neighbor’s morphology. It is argued that the tidal effects of the neighbor transform late type galaxies into early types. It is also hardly affected by the general tidal force field as indicated by its insensitivity to the large-scale background density.
3. At separations from the closest neighbor shorter than the virial radius, the probability of a galaxy to be an early morphological type continues to rise as ρ_n increases if the neighbor is an early type. The tidal, hydrodynamic, and radiative effects can result in this phenomenon. If the neighbor is a late type, however, the probability decreases as ρ_n increases and the galaxy tends to become a late type. The tide and the hot gas may be competing with the cold gas flowing from the neighbor in this circumstance.
4. The early type probability as a function of neighbor morphology, large- and small-scale densities, scales systematically as the luminosity changes over the magnitude range from $M_r = -19.0$ to -21.5 . The fraction increases sharply for $M_r \leq -21.5$.
5. It is found that galaxy luminosity depends sensitively on the local mass density due to the nearest neighbor. Isolated galaxies tend to be brighter and are more likely to be recent merger products. The merger-driven transformation of luminosity class can result in these phenomena.
6. We present a unified scenario that the galaxy morphology and luminosity classes change as galaxies approach one another and undergo a series of (mainly two-body) interactions and mergers. As the average interaction and merger rates are a function of the background density, the morphology–luminosity–density relation naturally arises under this scenario.

We were not able to study what happens to galaxy morphology and luminosity when the large-scale background density ρ_{20} exceeds the virial density. This is because the smoothing scale used to calculate ρ_{20} , which is $3.0_{-1.0}^{+1.4}h^{-1}$ Mpc, is larger than the size of the virial radius of clusters, which is typically about $1h^{-1}$ Mpc.

In a cluster environment, we expect to see morphology transform of late type galaxies when they are within the virial radius of the cluster.

We emphasize that one needs to take into account factors other than just one local density estimate when the effects of galaxy interactions in different environments are studied. In particular, the morphology of the closest neighbor is important when the separation is smaller than the virial radius of the neighbor. Without distinguishing the nearest neighbor by morphological type, the study of the effects of interactions on color, SFR, or morphology fraction will find almost a null signal because the early and late neighbors will tend to induce opposite trends. We will further investigate such effects of galaxy interactions in a forthcoming paper (Y.-Y. Choi et al. 2007 in preparation).

The authors thank H. B. Ahn, J. P. Ostriker, and M. S. Vogeley for helpful comments. CBP acknowledges the support of the Korea Science and Engineering Foundation (KOSEF) through the Astrophysical Research Center for the Structure and Evolution of the Cosmos (ARC-SEC). JRG is supported by NSF GRANT AST 04-06713.

Funding for the SDSS and SDSS-II has been provided by the Alfred P. Sloan Foundation, the Partic-

ipating Institutions, the National Science Foundation, the U.S. Department of Energy, the National Aeronautics and Space Administration, the Japanese Monbukagakusho, the Max Planck Society, and the Higher Education Funding Council for England. The SDSS Web Site is <http://www.sdss.org/>.

The SDSS is managed by the Astrophysical Research Consortium for the Participating Institutions. The Participating Institutions are the American Museum of Natural History, Astrophysical Institute Potsdam, University of Basel, Cambridge University, Case Western Reserve University, University of Chicago, Drexel University, Fermilab, the Institute for Advanced Study, the Japan Participation Group, Johns Hopkins University, the Joint Institute for Nuclear Astrophysics, the Kavli Institute for Particle Astrophysics and Cosmology, the Korean Scientist Group, the Chinese Academy of Sciences (LAMOST), Los Alamos National Laboratory, the Max-Planck-Institute for Astronomy (MPIA), the Max-Planck-Institute for Astrophysics (MPA), New Mexico State University, Ohio State University, University of Pittsburgh, University of Portsmouth, Princeton University, the United States Naval Observatory, and the University of Washington.

REFERENCES

- Adelman-McCarthy, J. K., et al. 2007, ApJS, submitted
Ahn, H., Park, C., & Choi, Y.-Y. 2007, ApJ, submitted
Balogh, M. L., et al. 2004a, MNRAS, 348, 1355
Balogh, M. L., Baldry, I. K., Nichol, R., Miller, C., Bower, R., & Glazebrook, K. 2004b, ApJ, 615, L101
Balogh, M. L., Navarro, J. F., & Morris, S. L. 2000, ApJ, 540, 113
Bell, E. F., Phleps, S., Somerville, R. S., Wolf, C., Borch, A., & Meisenheimer, K. 2006, ApJ, 652, 270
Bertola, F., Corsini, E. M., Vega Beltran, J. C., Pizzella, A., Sarzi, M., Cappellari, M., & Funes, J. G. 1999, ApJ, 519, 127
Binggeli, B., Sandage, A., & Tammann, G. A. 1985, AJ, 90, 1681
Binney, J., & Tremaine, S. 1987, Galactic Dynamics (Princeton: Princeton University Press), 438
Blanton, M. R., Eisenstein, D., Hogg, D. W., Schlegel, D. J., & Brinkmann, J. 2005a, ApJ, 629, 143
Blanton, M. R., et al. 2005b, ApJ, 129, 2562
Blanton, M. R., Lin, H., Lupton, R. H., Maley, F. M., Young, N., Zehavi, I., & Loveday, J. 2003a, AJ, 125, 2276
Blanton, M. R., et al. 2003b, AJ, 125, 2348
Choi, Y.-Y., Park, C., & Vogeley, M. S. 2007, ApJ, 658, 884 (Paper I)
Colless, M., et al. 2001, MNRAS, 328, 1039
Croton, D. J., et al. 2005, MNRAS, 356, 1155
Croton, D. J., Gao, L., & White, S. D. M. 2007, MNRAS, 374, 1303
Cullen, H., Alexander, P., Green, D. A., & Sheth, K. 2007, MNRAS, 376, 98
Dekel, A., & Birnboim, Y. 2006, MNRAS, 368, 2
Dressler, A. 1980, ApJ, 236, 351
Duc, P.-A., Brinks, E., Wink, J. E., & Mirabel, I. F. 1997, A&A, 326, 537
Elbaz, D., et al. 2007, A&A, 468, 33
Ellis, S. C., & O'Sullivan, E. 2006, MNRAS, 367, 627
Fukugita, M., Ichikawa, T., Gunn, J. E., Doi, M., Shimasaku, K., & Schneider, D. P. 1996, AJ, 111, 1748
Gao, L., Springel, V., & White, S. D. M. 2005, MNRAS, 363, 66
Gao, L., & White, S. D. M. 2007, MNRAS, 377, L5
Gnedin, O. Y. 2003, ApJ, 589, 752
Goto, T., et al. 2003, MNRAS, 346, 601
Gott, J. R., & Thuan, T. X. 1976, ApJ, 204, 649
Gott, J. R., & Rees, M. J. 1975, A&A, 45, 365
Gunn, J. E., et al. 2006, AJ, 131, 2332
Gunn, J. E., et al. 1998, AJ, 116, 3040
Gunn, J. E., & Gott, J. R. 1972, ApJ, 176, 1
Hamilton, A. J. S. & Tegmark, M. 2004, MNRAS, 349, 115
Hickson, P., Ninkov, Z., Huchra, J. P., & Mamon, G. A. 1984, 111, 367
Hogg, D. W., Finkbeiner, D. P., Schlegel, D. J., & Gunn, J. E. 2001, AJ, 122, 2129
Holmberg, E. 1958, Lund Medd. Astron. Obs. Ser. II, 136, 1
Hubble, E., & Humason, M. L., 1931, ApJ, 74, 43
Ivezic, Z., et al. 2004, AN, 325, 583
Keres, D., Katz, N., Weinberg, D. H., & Dave, R. 2005, MNRAS, 368, 2
Keel, W. C. 2004, AJ, 127, 1325
Kim, J., & Park, C. 2006, ApJ, 639, 600
Knapp, G. R., Turner, E. L., & Cuniffe, P. E. 1985, AJ, 90, 454
Karachentseva, V. E. 1973, Astrof. Issledovanija Byu. Spec. Ast. Obs., 8, 3
Larson, R. B., Tinsley, B. M., & Caldwell, C. N. 1980, ApJ, 237, 692
Lotz, J. M., et al. 2006, ApJ submitted (astro-ph/0602088)
Lupton, R. H., Gunn, J. E., Ivezic, Z., Knapp, G. R., Kent, S., & Yasuda, N. 2001, in ASP Conf. Ser. 238, Astronomical Data Analysis Software and Systems X, ed. F. R. Harnden, Jr., F. A. Primini, & H. E. Payne (San Francisco: ASP), 269
Marziani, P., Dultzin-Hacyan, D., D'Onofrio, M., & Sulentic, J. W. 2003, AJ, 125, 1897
Marcum, P. M., Aars, C. E., Fanelli, M. N. 2004, AJ, 127, 3213
Melnick, J., & Sargent, W. L. W. 1977, ApJ, 215, 401
Mihos, J. C., & Hernquist, L. 1994, ApJ, 425, 13
Moore, B., Katz, N., Lake, G., Dressler, A., & Oemler, A. 1996, Nature, 379, 613
Moss, C., Whittle, M. 2000, MNRAS, 317, 667
Oemler, A. 1974, ApJ, 194, 1
O'Sullivan, E., Forbes, D. A., & Ponman, R. J. 2001, MNRAS, 328, 461
Park, C., Choi, Y.-Y., Vogeley, M. S., Gott, J. R., & Blanton, M. R. 2007, ApJ, 658, 898 (Paper II)
Park, C., et al. 2005, ApJ, 633, 11
Park, C., & Choi, Y.-Y. 2005, ApJ, 635, L29
Pier, J. R., Munn, J. A., Hindsley, R. B., Hennessy, G. S., Kent, S. M., Lupton, R. H., & Ivezic, Z. 2003, AJ, 125, 1559
Postman, M., & Geller, M. 1984, ApJ, 281, 95
Prada, F., Gutierrez, C. M., Peletier, R. F., & McKeith, C. D. 1996, ApJ, 463, 9
Ramella, M., Giuricin, G., Mardirossian, F., & Mezzetti, M. 1987, A&A, 188, 1
Rojas, R. R., Vogeley, M. S., Hoyle, F., & Brinkmann, J. 2005, ApJ, 624, 571
Schechter, P. 1976, ApJ, 203, 297
Schlegel, D. J., Finkbeiner, D. P., & Davis, M. 1998, ApJ, 500, 525
Smith, J. A., et al. 2002, AJ, 123, 2121
Sotnikova, N. Y. 1990, in Proc. IAU Colloq. 124, Paired and Interacting Galaxies, ed Sulentic J. W., Keel W. C., & Tesco C. M., (NASA Conf. Publ. 3098), 717
Sofue, Y. 1994, ApJ, 423, 207
Stoughton, C., et al. 2002, AJ, 123, 485
Strauss, M. A., et al. 2002, AJ, 124, 1810
Tanaka, M., et al. 2004, AJ, 128, 2677

- Tegmark, M., et al. 2004, ApJ, 606,702
Toomre, A., & Toomre, J. 1972, ApJ, 178, 632
Tucker, D., et al. 2006, AN, in press
Varela, J., Moles, M., Marquez, I., Galletta, G., Masegosa, J., & Bettoni, D. 2004, A&A, 420, 873
Voges, W., et al. 1999, A&A, 349, 389
Wallin, J. F., & Stuart, B. V. 1992, ApJ, 399, 29
- Weinmann, S. M., van den Bosch, F. C., Yang, X., & Mo, H. J. 2006, MNRAS, 366, 2
Wechsler, R. H., Zentner, A. R., Bullock, J. S., Kravtsov, A. V., & Allgood, B. 2006, ApJ, 652, 71
York, D., et al. 2000, AJ, 120, 1579